Article

Facile Preparation of Porous Carbon Flake-Supported Nickel Nanoplates as Effective Catalysts for Methanol Electrooxidation

Ali Aldalbahi [1,*], Mohamed H. El-Newehy [1], Hany El-Hamshary [1], Edmund Samuel [2] and Sam S. Yoon [3]

1 Department of Chemistry, College of Science, King Saud University, Riyadh 11451, Saudi Arabia; melnewehy@ksu.edu.sa (M.H.E.-N.); helhamshary@ksu.edu.sa (H.E.-H.)
2 Energy Environment Policy and Technology, Graduate School of Energy and Environment (KU-KIST Green School), Korea University, Seoul 136-713, Korea; edsaedwin@rediffmail.com
3 School of Mechanical Engineering, Korea University, Seoul 136-713, Korea; skyoon@korea.ac.kr
* Correspondence: aaldalbahi@ksu.edu.sa

Abstract: Herein, we report a facile and efficient method for fabricating porous carbon flakes (PCFs)-supported nickel nanoplates (Ni NPs) as electrocatalysts for methanol oxidation in alkaline media. The catalyst was fabricated in one step using molten salt synthesis. Various techniques were used to characterize the morphology and composition of the Ni NPs@PCFs catalyst, and these revealed that the Ni NPs were dispersed finely across the PCFs with a highly crystalline structure. The Ni NPs@PCFs catalyst demonstrated high electrocatalytic activity for methanol oxidation (121 mA/cm^2 vs. Ag/AgCl), and it had an onset potential of 0.35 V. It also exhibited high stability in an alkaline electrolyte for the duration of the experiment (up to 2000 s).

Keywords: nickel nanoparticle; carbon flake; methanol oxidation; fuel cell

1. Introduction

Most modern energy and transportation systems still rely on fossil fuels, with oil being the most common. Alternative energy systems have received considerable attention in recent years as a means of alleviating pollution caused by fossil fuels. Because of their low cost, high energy density, and low operating temperature, fuel cells, notably direct methanol fuel cells (DMFCs), are promising energy sources for portable gadgets and electric cars [1–3]. To date, Pt- and Pd-based catalysts are generally considered the most common electrocatalysts for the methanol electro-oxidation reaction (MOR) because of their electrocatalytic activity and low overpotential [3–9]. However, the high cost of Pt- and Pd-based catalysts is one of the most significant barriers to the widespread use of methanol fuel cells as alternatives to fossil fuels [10–12]. Therefore, it is necessary to develop a low-cost electrocatalyst with good electrocatalytic activity toward methanol oxidation. Recently, Ni-based catalysts were recognized as promising alternatives to Pt and Pd metals because they have excellent catalytic activity for alcohols oxidation in alkaline media [13–15]. In general, the electrocatalytic activity and stability of Ni-based catalysts are affected by several factors, the most important of which are the surface structure and morphology of Ni, the morphology and structural arrangement of the support, and the extent of interaction between Ni and the support [15–17]. Significant research is devoted to developing effective strategies for improving the performance of Ni-based catalysts. Structural engineering design of the surface-active centers and increasing their density, as well as balancing the porosity and achieving a high surface area, are some of the strategies employed to improve the performance of Ni catalysts [18]. These approaches can improve charge transfer between the nickel catalyst surface and the conductive support. Nanostructuring Ni catalysts in the form of nanoparticles is an interesting engineering design for increasing the efficiency of the catalysts toward methanol oxidation [19–21]. However, pure Ni NPs often suffer from poisoning and leaching, resulting in rapid and irreversible deactivation [22,23]. Combining

Ni NPs with other transition metals or depositing Ni NPs on the surface of carbon materials can improve the electrocatalytic activity and durability. Thamer et al. fabricated Ni NPs on carbon nanofibers (CNFs) using electrospinning [24], where the electrocatalytic activity of the Ni@CNFs toward methanol oxidation was five times higher than that of Ni NPs. Sun et al. used a liquid-phase laser ablation approach to create Ni NPs supported by reduced graphene oxide (rGO) [25]. The Ni@rGO catalyst exhibited a high mass activity of 1600 mA/mg and excellent anti-poisoning characteristics. Javan et al. fabricated Ni NPs supported on carbon quantum dots using an electrodeposition technique [26]; the electrocatalytic activity of the Ni-NPs@CQDs was almost four times higher than that of Ni NPs. Wang et al. fabricated a honeycomb-like carbon framework as a support for Ni NPs by a multistep method, such as polymerization, carbonization, and impregnation/reduction, and utilized the supported NPs as an effective electrocatalyst for methanol oxidation [27]. However, the multi-steps and complexity of these methods still necessitate the development of facile and large-scale preparation methods, as well as low-cost carbon precursors.

In this study, we develop a novel, facile, low-cost, and large-scale method for synthesizing Ni NPs dispersed on porous carbon flakes (PCFs) as an effective electrocatalyst for methanol oxidation. The key to this method is the use of polyvinyl alcohol (PVA) and nickel acetate (NiAc) as sources of carbon and nickel, respectively. NiNPs@PCFs are fabricated through ball-milling followed by pyrolysis, without the need for any solvents or other chemicals. At 200 °C, the PVA melts, and the nickel ions are homogeneously dispersed inside the PVA structure. The subsequent pyrolysis of the PVA/NiAc composite carbonizes the polymer to PCFs and releases carbon monoxide, which reduces the Ni ions to Ni NPs in a single step. The prepared catalyst is attractive because PCFs have unique properties and can be fabricated on a large scale, making them suitable for industrial applications. Notably, the electrocatalytic activity and durability of the fabricated catalyst are much better than those of the Ni NPs@carbon material catalysts previously reported and fabricated using various methods.

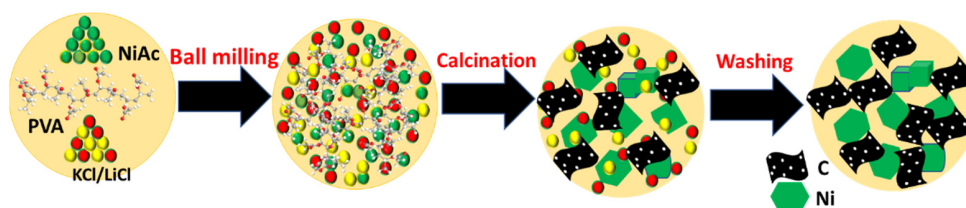## 2. Materials and Methods

2.1. Materials

Nickel acetate tetrahydrate (NiAc), lithium chloride, potassium chloride, poly(vinyl alcohol), methanol, Nafion (5% wt/v), and isopropanol were purchased from Sigma Aldrich and used without any further purification procedures.

2.2. Synthesis of NiNPs@PCFs

First, NiAc salt (0.5 g) was mixed with PVA (0.5 g) and then ground using a blender until a homogenized powder was obtained. NiAc/PVA was mixed with a molten salt of LiCl/KCl (45:55 by weight) at a ratio of 1:10, and the powders were homogenized by ball-milling. The powder combination was then placed in a quartz crucible and inserted into a tube furnace with a constant supply of argon gas. The mixture was calcined at 750 °C for 3.0 h at a heating rate of 3 °C/min. After 3.0 h, the heating stopped automatically, and the sample was cooled to 30 ± 5 °C while maintaining the flow of argon gas. The product containing the LiCl/KCl salt mixture was crushed into particles, and the salt was removed by washing with excess water, followed by filtration to obtain a black product. Finally, the product was dried in a vacuum oven at 60 °C overnight. Scheme 1 shows the molten salt synthesis for preparation the NiNPs@PCFs catalyst.

2.3. Characterization

The composition of the Ni NPs@PCFs was investigated by X-ray diffraction (XRD, Rigaku 2200, Rigaku-Corporation, Tokyo, Japan) analysis using Cu-Kα radiation (40 kV, 30 mA) and energy dispersive X-ray analysis (EDX). The morphology of NiNPs@PCFs was studied using field-emission scanning electron microscopy (SEM, JEOL-JSM-7401-F, Akishima, Tokyo, Japan) with an accelerating voltage of 5.0 kV and transmission electron microscopy (TEM, JEOL-JEM-2100, Akishima, Tokyo, Japan).

Scheme 1. Molten salt synthesis of Ni NPs@PCFSs.

3. Results and Discussion

3.1. Characterization

The morphology of the prepared catalyst was investigated using low- and high-magnification FESEM and TEM, as shown in Figure 1. From the low-magnification FESEM image, it is apparent that the prepared catalyst adopted a morphology comprising flaked and stacked compact layers (Figure 1a). The high-magnification FESEM image shows that the surface of the prepared catalyst was rough. The TEM image in Figure 1c shows Ni NPs with different shapes, such as hexagonal and cubic nanoplates. The TEM image reveals that the size of the nanoplates varied with their shape, where the hexagonal nanoplates ranged from 400 to 600 nm in width, whereas the width of the cubic nanoplates ranged from 200 to 300 nm. The high resolution TEM images of individual nanoplates of various shapes show clear lattice fringes. Figure 1d and Figure S1b show the crystalline nature of the Ni nanoplates with an interplanar spacing of 0.207 nm, which is consistent with the (111) crystal plane of the face center cubic (FCC) phase. The HRTEM image in Figure S1a also confirms that the Ni NPs are encapsulated in the PCFs.
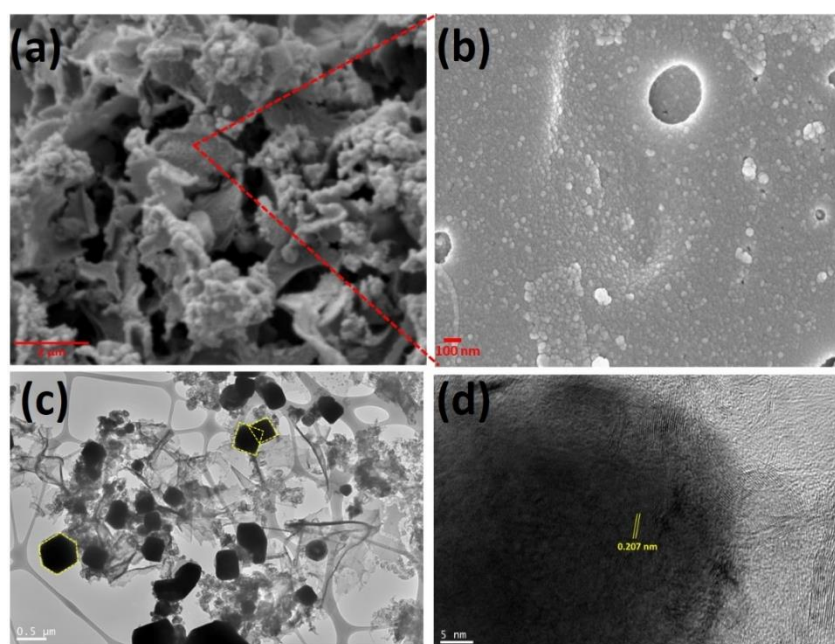

Figure 1. (**a**,**b**) Low- and high-magnification of FESEM images and (**c**,**d**) TEM and HR-TEM images of Ni NPs/PCFs.

The structural and crystalline arrangements of the prepared catalysts were investigated using EDX and XRD. Figure 2a display the EDX profiles of the NiNPs/PCFs, showing the presence of Ni and C with weight ratios of 24.3 and 75.77%, respectively. The XRD pattern of the prepared catalyst shows distinct sharp peaks of Ni at 44.32, 51.67, and 76.30°, confirming the crystallinity of the nickel nanoplates (JCPDS No. 04-0850). All the three peaks for the nanoplates are at nearly identical positions and are in good agreement with the (111), (200), and (220) lattice planes reported for Ni phase nanoplates. This showed that

the resulting Ni NPs are pure face center cubic nickel (FCC). No obvious peaks of nickel oxides and hydroxides were detected due to the complete reduction of nickel during the pyrolysis process by carbon monoxide that produces from the decomposition of the PVA. However, some weak peaks appear at 28.2° and 40.36°, which are attributed to molten salt residual entrapped between graphite layers.
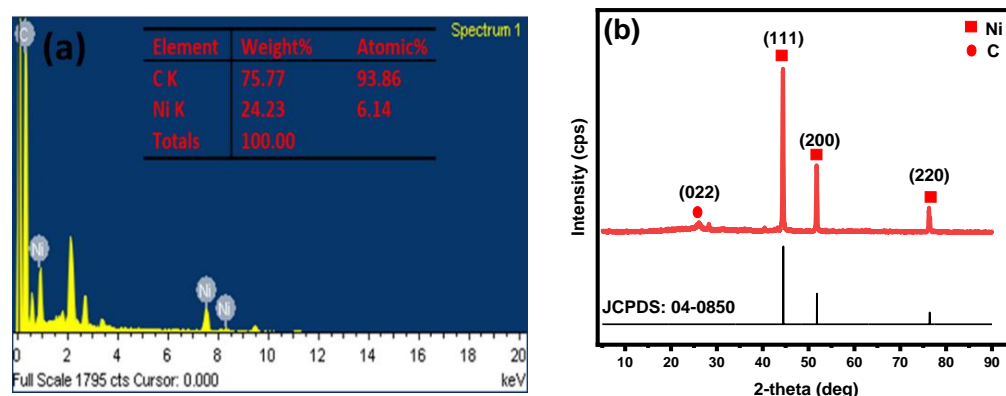

Figure 2. (**a**) EDX profiles and (**b**) XRD spectra of NiNPs@PCFs.

Thermogravimetry/differential thermal analysis (TGA/DTA) was used to investigate the thermal behavior of NiAc, PVA, and NiAc/PVA (1:1 *wt/wt*). Analyzing the thermal degradation of the starting materials is an important step in determining the optimal conditions for preparing the catalyst. NiAc underwent thermal decomposition in three main steps, as shown in the DTA curve (Figure 3). The first step spanned the range of 50–160 °C and reached a maximum of 110 °C, corresponding to the loss of physically and chemically bound water molecules. The second step took place after the dehydration process and occurred in the range of 260–380 °C, peaking at 350 °C. This step corresponds to the decomposition of the dehydrated intermediate into NiO. The third step occurred in a limited range between 380 and 435 °C, peaking at 398 °C, corresponding to the reduction of nickel oxide to nickel particles doped with residual carbon impurities. PVA underwent thermal decomposition into carbon in two main steps, where the residual carbon was 5%. The main step occurred at 350 °C, corresponding to the breakdown of PVA into polyene structures by a dehydration process, with 70% weight loss. The second step at 470 °C is associated with the decomposition and carbonization of the polyene structure into amorphous carbon (residual weight 5%). The PVA/NiAc blend underwent thermal degradation in four steps, as shown in Figure 3. The first step spanning 50–140 °C with a peak at 97 °C, corresponds to the loss of physically adsorbed water (moisture) from the sample. The second peak between 236 and 392 °C is attributed to the degradation of the PVA backbone. The third peak occurred in a narrow range of 400 to 440 °C and corresponds to the dissociation of nickel carbonate into nickel oxide. The final peak at 400–480 °C is attributed to the reduction of nickel oxide to nickel. The residual weight of the PVA/NiAc sample at 600 °C was 18%, which is higher than the residual weight of PVA and less than the residual weight of NiAc. The residual weight of the PVA/NiAc sample at 600 °C was 18%, which is higher than the residual weight of the PVA (5%) and less than the residual weight of NiAc (27%). Based on the TGA/DTA analysis, a temperature above 550 °C is suitable for the calcination step in the preparation of the catalyst.
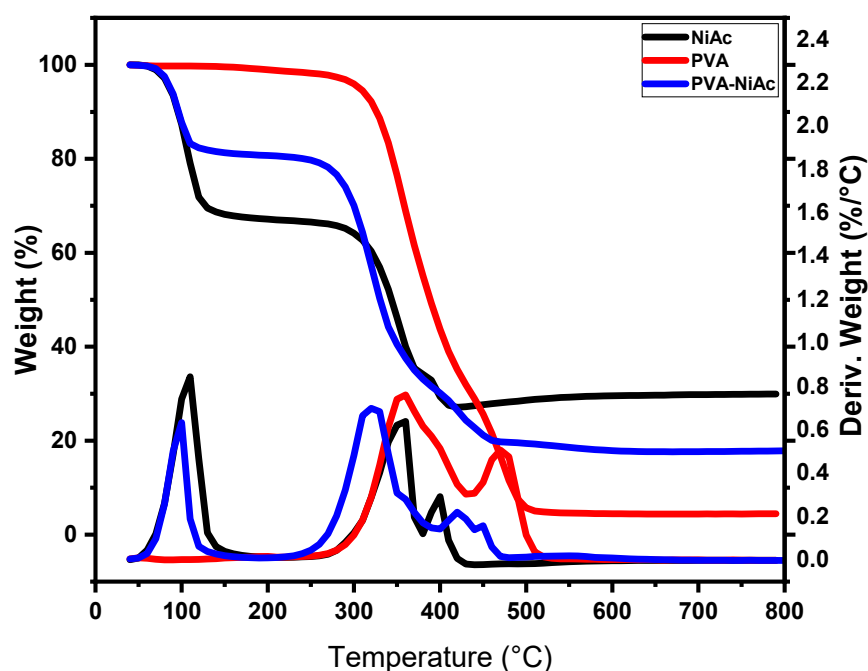
Figure 3. TGA/DTA analysis of NiAc, PVA, and PVA/NiAc blend.

3.2. Electrochemical Measurements

Ni-based catalysts are effective for alcohol oxidation because they form a thicker layer of NiOOH on their surface [24,28]. This layer can be produced by increasing the number of potential sweeps in an alkaline medium, where the formation of the hydroxyl ion is enhanced by reacting with the $Ni(OH)_2$ layer according to Equations (1) and (2).

$$Ni + 2OH^- \rightarrow Ni(OH)_2 + 2e^- \tag{1}$$

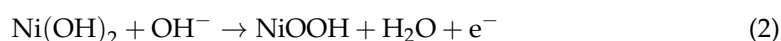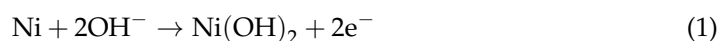$$Ni(OH)_2 + OH^- \rightarrow NiOOH + H_2O + e^- \tag{2}$$

Figure 4 show the CV profiles of the NiNPs@PCFs, which were acquired over 10 cycles in 1.0 M KOH in the anodic direction, followed by a reversal in the cathodic direction back to 1.0 V and measurement at a scan rate of 50 mV/s. The sharp anodic peak at 0.38 V is related to the creation of a layer of NiOOH by oxidation of the Ni NPs in alkaline media, and the broad cathodic peak at ~0.24 V is due to the conversion of NiOOH to $Ni(OH)_2$ by reduction. Figure 4 also show that increasing the number of potential sweeps led to an increase in the current density of the anodic peak because the hydroxyl ion interacts with the $Ni(OH)_2$ layer and produces a thin layer of NiOOH.

Figure 5 show the effect of the methanol concentration on the electrocatalytic performance of the prepared electrocatalyst. Figure 5a–f display the CV curves of the Ni NPs@PCFs catalyst in various concentrations of methanol (from 0.1 to 4.0 M), scanned in the potential window from 0.20 to 0.80 V at a scan rate of 0.05 V/s. The current density increased from 28 to 121 mA/cm^2 as the concentration increased from 0.1 to 2 M, followed by a slight decrease at higher concentrations. The linear increase in the current density at lower concentrations is attributed to a diffusion-controlled process that plays an important role at this range of concentrations. Furthermore, at low methanol concentrations (0.1 and 0.5 M), two anodic peaks were observed: I_{ap} (attributed to the oxidation of $Ni(OH)_2$ to NiOOH) and II_{ap} (designated as the oxidation of methanol), as shown in Figure 5a,b, respectively. At methanol concentrations higher than 0.5 M, the I_{ap} peak disappeared and overlapped with the II_{ap} peak, with a noticeable increase in the current density. Notably, the maximum of the II_{ap} peak shifted to higher potential with increasing methanol concentration, as shown in Figure 5h. The decrease in current density at concentrations above 2.0 M can be attributed to an increase in the viscosity of the electrolyte, which impedes

the diffusion of methanol molecules on the surface of the catalyst [15]. This can also be attributed to the fact that the number of reactant (methanol) molecules and undecomposed intermediates on the surface of the catalyst was higher than the number of active sites on the catalyst surface, which slowed the reaction kinetics when the methanol concentration was higher than 2.0 M [29].

The effect of scan rate on the CV response of the NiNPs@PCFs catalyst was also evaluated, and the results are presented in Figure 6. The cathodic and anodic peak current densities increased with increasing scan rates, and both showed a linear response to the scan rate in the range of 10 to 300 mV/s. The plot of the anodic and cathodic peak current densities versus the square root of the scan rate was linear, as shown in Figure 6b. This result confirms that the diffusion-controlled mechanism is the dominant mechanism for methanol oxidation on the surface of the NiNPs@PCFs catalyst. Furthermore, the peak potentials for methanol oxidation on the surface of the NiNPs@PCFs catalyst shifted to higher values as the scan rate increased, indicating that methanol oxidation on the NiNPs@PCFs surface is an irreversible electrode process.

The stability of the NiNPs@PCFs electrocatalyst over a prolonged period in the methanol oxidation reaction was examined using chronoamperometry. Figure 7 display the chronoamperograms acquired in a solution of 2.0 M CH_3OH/1.0 M KOH for 2000 s at applied potentials of 0.5 and 0.7 V. A rapid decrease in the current density was observed at the beginning of the MOR because the number of methanol molecules interacting with the surface of the electrocatalyst in the first few seconds was less than the number of active sites. The current density initially decreased and reached a steady state within approximately 100 s at a potential of 0.4 V but became unstable within 500 s at a potential of 0.7 V. After completing a stability test, it was found that the prepared catalyst kept its morphology as shown in Figure S2.
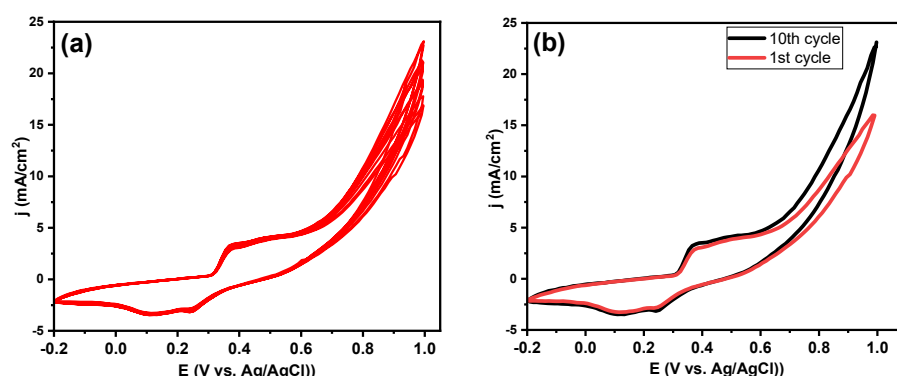

Figure 4. (**a**) CV curve acquired over ten cycles and (**b**) 1st and 10th cycle in 1.0 M KOH at a scan rate of 50 mV/s.
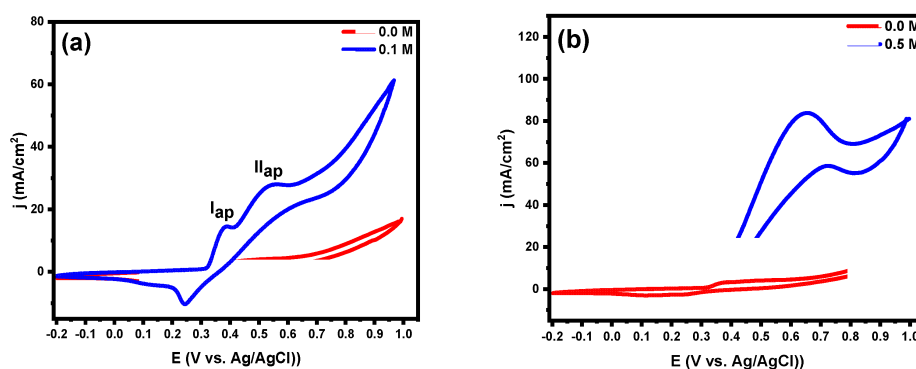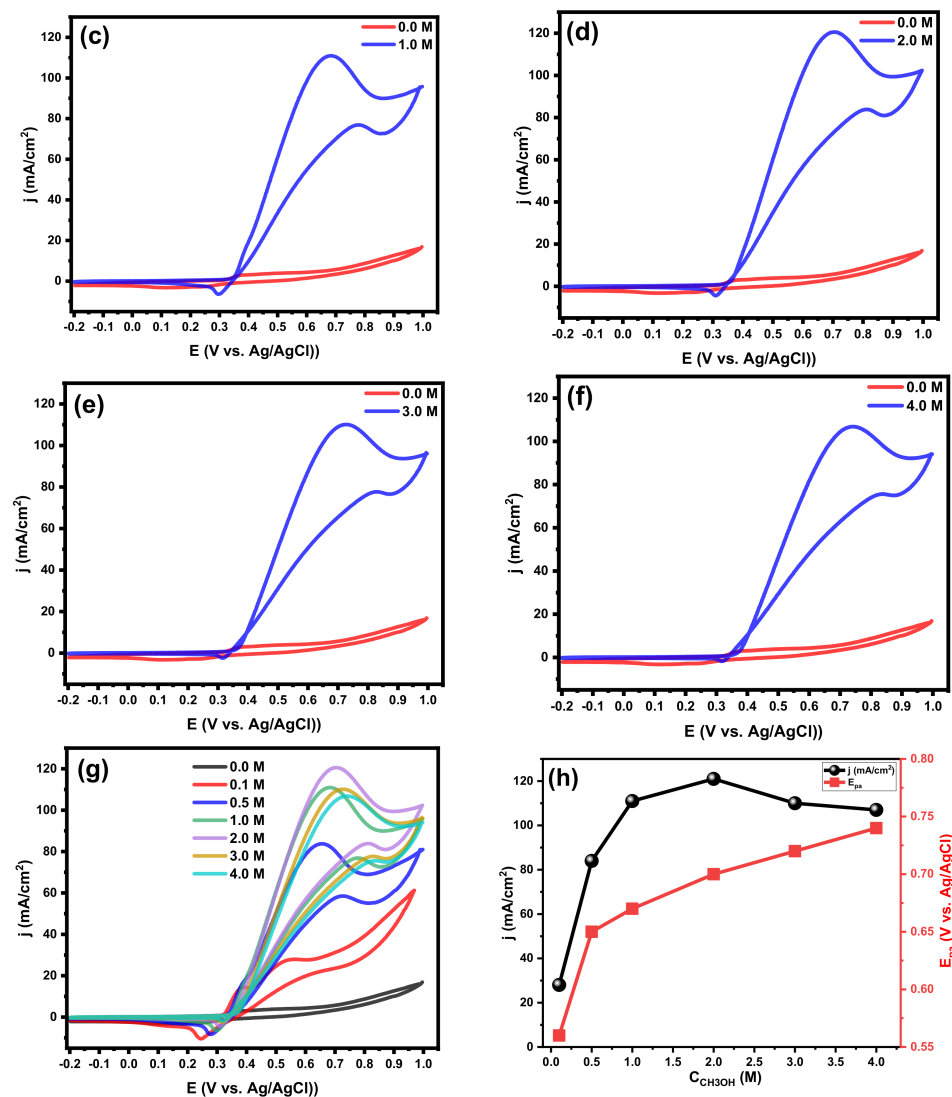

Figure 5. *Cont.*

Figure 5. (**a–f**) CV curves of Ni NPs@PCFs catalyst in 1.0 M KOH + various CH$_3$OH concentrations at a scan rate of 50 mV/s and (**h**) CH$_3$OH concentration effect on E_{pa} and current density.

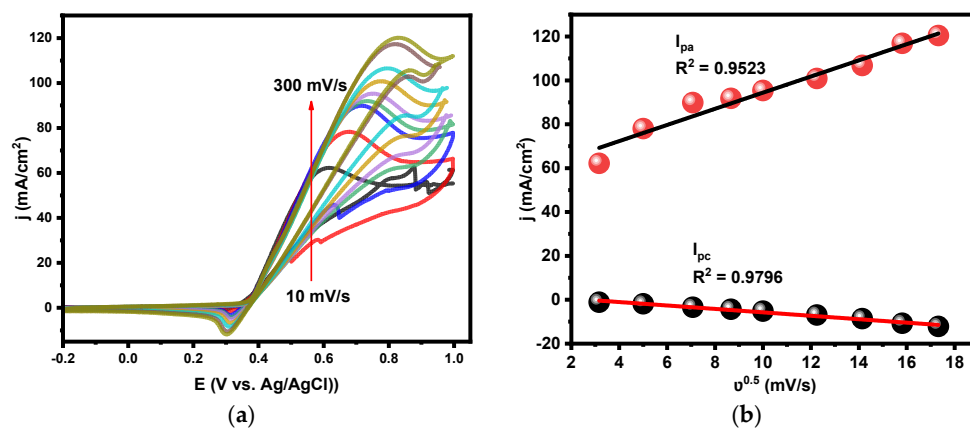**Figure 6.** (**a**) CV curves of NiNPs@PCFs in the presence of 0.5 M CH$_3$OH and 1.0 M KOH at different potential scan rates and (**b**) linear fitting of the cathodic (I$_{cp}$) and anodic (I$_{pa}$) peak current densities vs. the square roots of the scan rates.
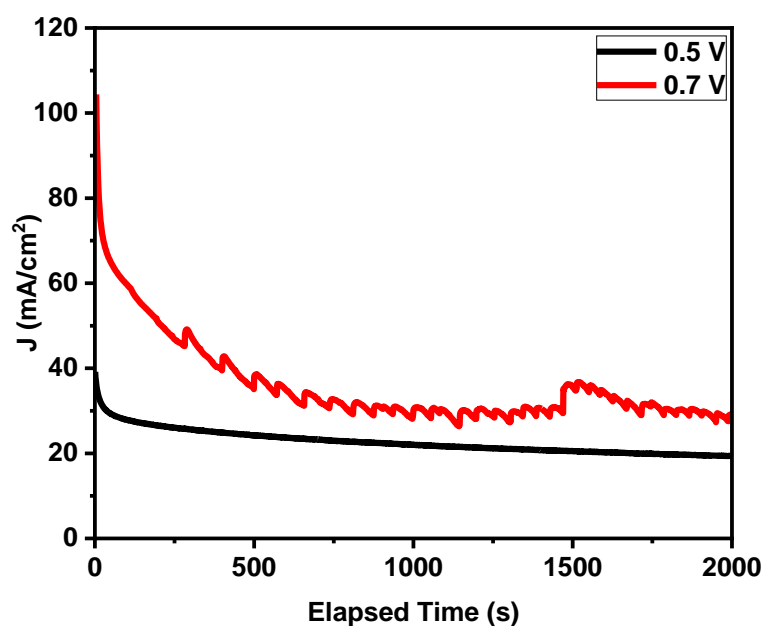
Figure 7. Chronoamperogram for CH_3OH electrooxidation on NiNPs@PCFs catalyst at potential of 0.4 and 0.7 V in 2.0 M CH_3OH + 1.0 M KOH.

The electrocatalytic activity of the prepared catalyst can be explored when comparing its peak current density and onset potential with the results reported for previously investigated nickel-based catalysts [25,26,30–35] as listed in Table 1. The onset potential value of the prepared NiNPs@PCFs catalyst was 0.35 V and more negative than that shown for NiNPs/RCQDs [26], Ni NPs@r-GO [25], and Ni NPs/Vulcan carbon black [31]. In addition, as compared to nickel-based catalysts, NiNPs@PCFs provided a significantly higher oxidation current density (121 mA/cm^2) than nickel nanoparticles/carbon nitride (55 mA/cm^2) [30], nickel nanoparticles/Vulcan carbon (30 mA/cm^2) [31], NiSe/CNFs (67 mA/cm^2) [32], NiCo bimetallic/graphene (75 mA/cm^2) [33], NiCu bimetallic/graphene (84 mA/cm^2) [35], Ni NPs@r-GO (20 mA/cm^2) [25], and NiNPs/RCQDs (32 mA/cm^2) [26]. Moreover, the prepared catalyst is characterized by its facile preparation, without the need for inorganic solvents, and the possibility of producing it commercially.

Table 1. Comparison of the catalytic activity of Ni-based catalysts toward methanol oxidation in alkaline media.

Electrocatalyst	Conditions		J (mA/cm^2)	Onset Potential	Ref.
	Scan Rate	Electrolyte CH_3OH/KOH			
Ni/CN	50	3.0M/1.0 M	55	0.35 V vs. Ag/AgCl	[30]
Ni/C-30	50	0.4 M/0.5 M	30	0.5 V vs. Hg/HgO	[31]
NiSn/CNFs	50	1.0 M/1.0 M	67	0.315 V vs. Ag/AgCl	[32]
Ni$_{0.2}$Co$_{0.2}$/graphene	50	3.0 M/1.0 M	75	0.35 V vs. Ag/AgCl	[33]
NiO/CNT	50	0.5 M/1.0 M	128	0.34 V vs. Ag/AgCl	[34]
Ni$_{0.75}$Cu$_{0.25}$	50	0.5 M/1.0 M	84	0.33 V vs. Ag/AgCl	[35]

Table 1. *Cont.*

Electrocatalyst	Conditions		J (mA/cm^2)	Onset Potential	Ref.
	Scan Rate	Electrolyte CH$_3$OH/KOH			
Ni NPs@r-GO	10	0.08 M/0.1 M	20	0.536 V vs. Ag/AgCl	[25]
NiNPs/RCQDs	50	2.0 M/1.0 M	32	0.56 V vs. Ag/AgCl	[26]
NiNPs@PCFs	50	2.0 M/1.0 M	121	0.35 V vs. Ag/AgCl	This study

4. Conclusions

Ni NPs supported on PCFs were prepared as electrocatalysts for methanol oxidation by a facile and efficient molten salt method. FESEM and TEM imaging showed that the prepared catalyst comprised PCFS sheets with distributed Ni nanoplates. The strong interfacial contact in the encapsulated PCFs nanostructure of the Ni NPs prevented the corrosion and dissolution of the Ni NPs during methanol oxidation. The prepared catalyst showed excellent electrocatalytic activity toward methanol oxidation in an alkaline medium, affording a current density of 121 mA/cm^2 and onset potential of 0.35 V vs. Ag/AgCl, along with good long-term stability. Our synthesis method is not limited to Ni NPs@PCFs and can be used to create a wide range of metal NPs/porous carbon framework catalysts. This accomplishment represents a significant step forward in the fabrication of non-precious metal-based electrocatalysts on a large scale using an uncomplicated process, paving the way for the development of low-cost fuel cells.

Supplementary Materials: The following supporting information can be downloaded at: https://www.mdpi.com/article/10.3390/catal12050556/s1, Figure S1: HRTEM images (a) 20nm; (b) 5 nm of Ni NPs@PCFs; Figure S2: TEM images of NiNPs@PCFs after test durability.

Author Contributions: Conceptualization, A.A. and M.H.E.-N.; methodology, A.A.; M.H.E.-N.; H.E.-H.; formal analysis, A.A.; M.H.E.-N.; investigation, M.H.E.-N.; H.E.-H.; E.S. and S.S.Y.; resources, M.H.E.-N.; H.E.-H.; E.S. and S.S.Y.; data curation, M.H.E.-N.; H.E.-H.; E.S. and S.S.Y.; writing—original draft preparation, A.A and M.H.E.-N.; writing—review and editing, M.H.E.-N.; H.E.-H.; E.S. and S.S.Y.; project administration, A.A.; funding acquisition, A.A. All authors have read and agreed to the published version of the manuscript.

Data Availability Statement: Not applicable.

Conflicts of Interest: The authors declare no conflict of interest.

References

1. Xia, Z.; Zhang, X.; Sun, H.; Wang, S.; Sun, G. Recent advances in multi-scale design and construction of materials for direct methanol fuel cells. *Nano Energy* **2019**, *65*, 104048. [CrossRef]
2. Zhao, X.; Yin, M.; Ma, L.; Liang, L.; Liu, C.; Liao, J.; Lu, T.; Xing, W. Recent advances in catalysts for direct methanol fuel cells. *Energy Environ. Sci.* **2011**, *4*, 2736–2753. [CrossRef]
3. Bianchini, C.; Shen, P.K. Palladium-Based Electrocatalysts for Alcohol Oxidation in Half Cells and in Direct Alcohol Fuel Cells. *Chem. Rev.* **2009**, *109*, 4183–4206. [CrossRef]
4. Thamer, B.M.; El-Newehy, M.H.; Barakat, N.A.M.; Al-Deyab, S.S.; Kim, H.Y. Preparation of zero-valent Co/N-CNFs as an immobilized thin film onto graphite disc for methanol electrooxidation. *Fibers Polym.* **2017**, *18*, 696–705. [CrossRef]
5. Zu, X.; Thamer, B.M.; Abdulhameed, M.M.; El-Newehy, M.H. Tragacanth Gum Hydrogel-Derived Trimetallic Nanoparticles Supported on Porous Carbon Catalyst for Urea Electrooxidation. *Gels* **2022**, *8*, 292. [CrossRef]

6. Hanifah, M.F.R.; Jaafar, J.; Othman, M.H.D.; Ismail, A.F.; Rahman, M.A.; Yusof, N.; Aziz, F.; Rahman, N.A. One-pot synthesis of efficient reduced graphene oxide supported binary Pt-Pd alloy nanoparticles as superior electro-catalyst and its electro-catalytic performance toward methanol electro-oxidation reaction in direct methanol fuel cell. *J. Alloys Compd.* **2019**, *793*, 232–246. [CrossRef]
7. Eris, S.; Daşdelen, Z.; Sen, F. Enhanced electrocatalytic activity and stability of monodisperse Pt nanocomposites for direct methanol fuel cells. *J. Colloid Interface Sci.* **2018**, *513*, 767–773. [CrossRef]
8. Yang, H.; Geng, L.; Zhang, Y.; Chang, G.; Zhang, Z.; Liu, X.; Lei, M.; He, Y. Graphene-templated synthesis of palladium nanoplates as novel electrocatalyst for direct methanol fuel cell. *Appl. Surf. Sci.* **2019**, *466*, 385–392. [CrossRef]
9. Yaqoob, L.; Noor, T.; Iqbal, N. Recent progress in development of efficient electrocatalyst for methanol oxidation reaction in direct methanol fuel cell. *Int. J. Energy Res.* **2021**, *45*, 6550–6583. [CrossRef]
10. Thamer, B.M.; El-Newehy, M.H.; Al-Deyab, S.S.; Abdelkareem, M.A.; Kim, H.Y.; Barakat, N.A.M. Cobalt-incorporated, nitrogen-doped carbon nanofibers as effective non-precious catalyst for methanol electrooxidation in alkaline medium. *Appl. Catal. A Gen.* **2015**, *498*, 230–240. [CrossRef]
11. Baruah, B.; Deb, P. Performance and application of carbon-based electrocatalysts in direct methanol fuel cell. *Mater. Adv.* **2021**, *2*, 5344–5364. [CrossRef]
12. Sealy, C. The problem with platinum. *Mater. Today* **2008**, *11*, 65–68. [CrossRef]
13. An, Y.; Ijaz, H.; Huang, M.; Qu, J.; Hu, S. The one-pot synthesis of CuNi nanoparticles with a Ni-rich surface for the electrocatalytic methanol oxidation reaction. *Dalt. Trans.* **2020**, *49*, 1646–1651. [CrossRef] [PubMed]
14. Abbas, M.; Abdel Hameed, R.M.; Al-Enizi, A.M.; Thamer, B.M.; Yousef, A.; El-Newehy, M.H. Decorated carbon nanofibers with mixed nickel−manganese carbides for methanol electro-oxidation in alkaline solution. *Int. J. Hydrogen Energy* **2021**, *46*, 6494–6512. [CrossRef]
15. Thamer, B.M.; El-Newehy, M.H.; Barakat, N.A.M.; Abdelkareem, M.A.; Al-Deyab, S.S.; Kim, H.Y. In-situ synthesis of Ni/N-doped CNFs-supported graphite disk as effective immobilized catalyst for methanol electrooxidation. *Int. J. Hydrogen Energy* **2015**, *40*, 14845–14856. [CrossRef]
16. Bu, X.; Wei, R.; Cai, Z.; Quan, Q.; Zhang, H.; Wang, W.; Li, F.; Yip, S.P.; Meng, Y.; Chan, K.S.; et al. More than physical support: The effect of nickel foam corrosion on electrocatalytic performance. *Appl. Surf. Sci.* **2021**, *538*, 147977. [CrossRef]
17. Yuda, A.; Ashok, A.; Kumar, A. A comprehensive and critical review on recent progress in anode catalyst for methanol oxidation reaction. *Catal. Rev.* **2020**, *64*, 126–228. [CrossRef]
18. Zhang, J.; Zhang, Q.; Feng, X. Support and Interface Effects in Water-Splitting Electrocatalysts. *Adv. Mater.* **2019**, *31*, 1808167. [CrossRef]
19. Zhu, H.; Wang, J.; Liu, X.; Zhu, X. Three-dimensional porous graphene supported Ni nanoparticles with enhanced catalytic performance for Methanol electrooxidation. *Int. J. Hydrogen Energy* **2017**, *42*, 11206–11214. [CrossRef]
20. Ferdowsi, G.S.; Seyedsadjadi, S.A.; Ghaffarinejad, A. Ni nanoparticle modified graphite electrode for methanol electrocatalytic oxidation in alkaline media. *J. Nanostruct. Chem.* **2014**, *5*, 17–23. [CrossRef]
21. Ren, L.; Hui, K.S.; Hui, K.N. Self-assembled free-standing three-dimensional nickel nanoparticle/graphene aerogel for direct ethanol fuel cells. *J. Mater. Chem. A* **2013**, *1*, 5689–5694. [CrossRef]
22. Oshchepkov, A.G.; Bonnefont, A.; Pronkin, S.N.; Cherstiouk, O.V.; Ulhaq-Bouillet, C.; Papaefthimiou, V.; Parmon, V.N.; Savinova, E.R. Nanostructured nickel nanoparticles supported on vulcan carbon as a highly active catalyst for the hydrogen oxidation reaction in alkaline media. *J. Power Sources* **2018**, *402*, 447–452. [CrossRef]
23. Barakat, N.A.M.; Motlak, M.; Kim, B.S.; El-Deen, A.G.; Al-Deyab, S.S.; Hamza, A.M. Carbon nanofibers doped by NixCo1−x alloy nanoparticles as effective and stable non precious electrocatalyst for methanol oxidation in alkaline media. *J. Mol. Catal. A Chem.* **2014**, *394*, 177–187. [CrossRef]
24. Thamer, B.M.; El-Newehy, M.H.; Barakat, N.A.M.; Abdelkareem, M.A.; Al-Deyab, S.S.; Kim, H.Y. Influence of Nitrogen doping on the Catalytic Activity of Ni-incorporated Carbon Nanofibers for Alkaline Direct Methanol Fuel Cells. *Electrochim. Acta* **2014**, *142*, 228–239. [CrossRef]
25. Sun, H.; Ye, Y.; Liu, J.; Tian, Z.; Cai, Y.; Li, P.; Liang, C. Pure Ni nanocrystallines anchored on rGO present ultrahigh electrocatalytic activity and stability in methanol oxidation. *Chem. Commun.* **2018**, *54*, 1563–1566. [CrossRef]
26. Javan, H.; Asghari, E.; Ashassi-Sorkhabi, H.; Moradi-Haghighi, M. Nickel nanoparticles decorated on carbon quantum dots as a novel non-platinum catalyst for methanol oxidation; a green, low-cost, electrochemically-synthesized electrocatalyst. *Chem. Eng. Sci.* **2020**, *217*, 115534. [CrossRef]
27. Wang, J.; Zhao, Q.; Hou, H.; Wu, Y.; Yu, W.; Ji, X.; Shao, L. Nickel nanoparticles supported on nitrogen-doped honeycomb-like carbon frameworks for effective methanol oxidation. *RSC Adv.* **2017**, *7*, 14152–14158. [CrossRef]
28. Vuković, M. Voltammetry and anodic stability of a hydrous oxide film on a nickel electrode in alkaline solution. *J. Appl. Electrochem.* **1994**, *24*, 878–882. [CrossRef]
29. Theres, G.S.; Velayutham, G.; Suresh, C.; Krishnan, P.S.; Shanthi, K. Promotional effect of Ni–Co/ordered mesoporous carbon as non-noble hybrid electrocatalyst for methanol electro-oxidation. *J. Appl. Electrochem.* **2020**, *50*, 639–653. [CrossRef]
30. Pieta, I.S.; Rathi, A.; Pieta, P.; Nowakowski, R.; Hołdynski, M.; Pisarek, M.; Kaminska, A.; Gawande, M.B.; Zboril, R. Electrocatalytic methanol oxidation over Cu, Ni and bimetallic Cu-Ni nanoparticles supported on graphitic carbon nitride. *Appl. Catal. B Environ.* **2019**, *244*, 272–283. [CrossRef]

31. Abdel Hameed, R.M.; El-Sherif, R.M. Microwave irradiated nickel nanoparticles on Vulcan XC-72R carbon black for methanol oxidation reaction in KOH solution. *Appl. Catal. B Environ.* **2015**, *162*, 217–226. [CrossRef]

32. Barakat, N.A.M.; Al-Mubaddel, F.S.; Rezual Karim, M.; Alrashed, M.; Yong Kim, H. Influence of Sn content on the electrocatalytic activity of NiSn alloy nanoparticles-incorporated carbon nanofibers toward methanol oxidation. *Int. J. Hydrogen Energy* **2018**, *43*, 21333–21344. [CrossRef]

33. Barakat, N.A.M.; Motlak, M. CoxNiy-decorated graphene as novel, stable and super effective non-precious electro-catalyst for methanol oxidation. *Appl. Catal. B Environ.* **2014**, *154–155*, 221–231. [CrossRef]

34. Tong, X.; Qin, Y.; Guo, X.; Moutanabbir, O.; Ao, X.; Pippel, E.; Zhang, L.; Knez, M. Enhanced Catalytic Activity for Methanol Electro-oxidation of Uniformly Dispersed Nickel Oxide Nanoparticles—Carbon Nanotube Hybrid Materials. *Small* **2012**, *8*, 3390–3395. [CrossRef]

35. Cui, X.; Xiao, P.; Wang, J.; Zhou, M.; Guo, W.; Yang, Y.; He, Y.; Wang, Z.; Yang, Y.; Zhang, Y.; et al. Highly Branched Metal Alloy Networks with Superior Activities for the Methanol Oxidation Reaction. *Angew. Chem. Int. Ed.* **2017**, *56*, 4488–4493. [CrossRef]